Supporting Information

Bulky Ligands Shape the Separation between the Large Spin Carriers to Condition Field-induced Slow Magnetic Relaxation

Jedrzej Kobylarczyk,[a] Michał Liberka,[a] Piotr Konieczny,*[b] Stanisław Baran,[c] Maciej Kubicki,[d] Tomasz Korzeniak,[a] Robert Podgajny*,[a]

[a]*Faculty of Chemistry, Jagiellonian University, Gronostajowa 2, 30-387 Kraków, Poland*

[b]*Institute of Nuclear Physics PAN, Radzikowskiego 152, 31-342 Kraków, Poland*

[c]*Department of Solid State Physics, Marian Smoluchowski Institute of Physics, Faculty of Physics, Astronomy and Applied Computer Science of the Jagiellonian University, Łojasiewicza 11, 30-348 Kraków, Poland*

[d]*Faculty of Chemistry, Adam Mickiewicz University, Umultowska 89b, 61-614 Poznań*

TABLE OF CONTENTS

I. Structural description

Table S1. Selected parameters and structural data of compounds **1**, **1a** and **2**

Compound	**1**	**1a**	**2**
Empirical formula	$C_{219}H_{230}Mn_9N_{64}O_{22}W_6$	$C_{222}H_{280}Mn_9N_{64}O_{14}W_6$	$C_{277}H_{159}Mn_9N_{64}O_{43}W_6$
Formula weight	5708.22	5666.64	6669.23
T, K	100	100	117
Crystal system	triclinic	triclinic	Triclinic
Space group	P-1	P-1	P-1
a, Å	20.2710(13)	16.0808(10)	24.8236(9)
b, Å	20.3406(13)	20.4138(10)	25.1491(8)
c, Å	20.3665(13)	20.5125(13)	25.8948(9)
α, deg	93.7930(10)	82.386(5)	89.0040(10)
β, deg	98.1180(10)	74.694(5)	83.0100(10)
γ, deg	96.5350(10)	86.907(4)	87.2110(10)
V, Å^3	8230.5(9)	6436.3(7)	16025.7(10)
Z	1	1	2
ρ_{calc}, g/cm^3	1.152	1.462	1.382
Abs coefficient, mm^{-1}	2.471	3.157	2.555
F [000]	2837.0	2841.0	6564.0
Crystal size, mm^3	0.25 × 0.21 × 0.09	0.15× 0.15 × 0.12	0.26 × 0.18 × 0.11
2θ range, deg	4.59 to 50.054	6.042 to 50.000	4.508 to 50.056
Index range	-24 ≤ h ≤ 24, -24 ≤ k ≤ 24, -24 ≤ l ≤ 24	-19 ≤ h ≤ 19, -24 ≤ k ≤ 24, -24 ≤ l ≤ 24	-29 ≤ h ≤ 29, -29 ≤ k ≤ 29, -30 ≤ l ≤ 30
Reflections collected	97439	112115	201199
Independent reflections	29042	22598	56317
R_{int}	0.0694	0.1213	0.0922
Data / restraints / parameters	29042/148/1654	22598/820/1455	56317/125/3475
Goodness-of-fit on F^2	1.019	1.089	1.015
Final R indices [I>=2σ (I)]	R_1 = 0.0501, wR_2 = 0.1242	R_1 = 0.0667, wR_2 = 0.1166	R_1 = 0.0553, wR_2 = 0.1233
R indices (all data)	R_1 = 0.0844, wR_2 = 0.1433	R_1 = 0.1187, wR_2 = 0.1318	R_1 = 0.0942, wR_2 = 0.1396
Largest diff peak/hole, e·Å^3	2.25/-1.15	2.52/-1.35	3.07 / -1.28

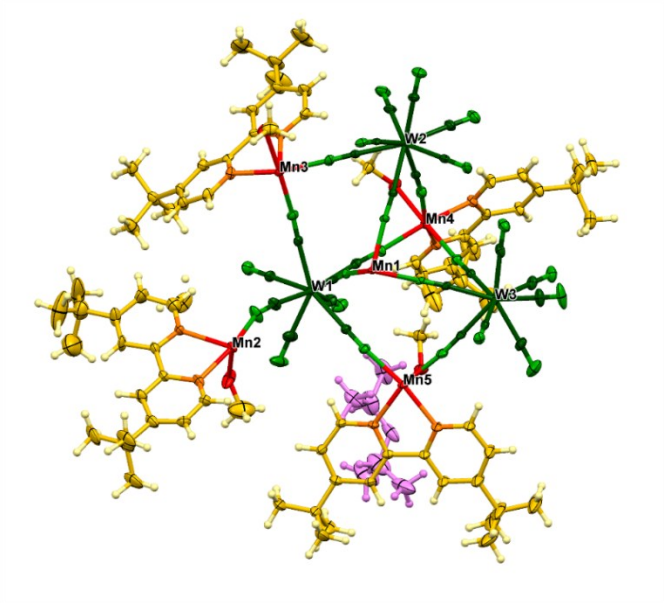

Figure S1. Asymmetric unit of **1** with atom labelling scheme for metal ions. Atoms spheres are shown with 50% probability ellipsoids. Colours: W, dark green; Mn, red; C of cyanide ligands, green; N of cyanide ligands, light green; N of Bu^t_2bpy ligand, orange, C of Bu^t_2bpy, intense yellow ; H, pale yellow; O of MeOH molecules red; C of MeOH molecules, intense yellow; iPr-O-iPr molecule, magenta.

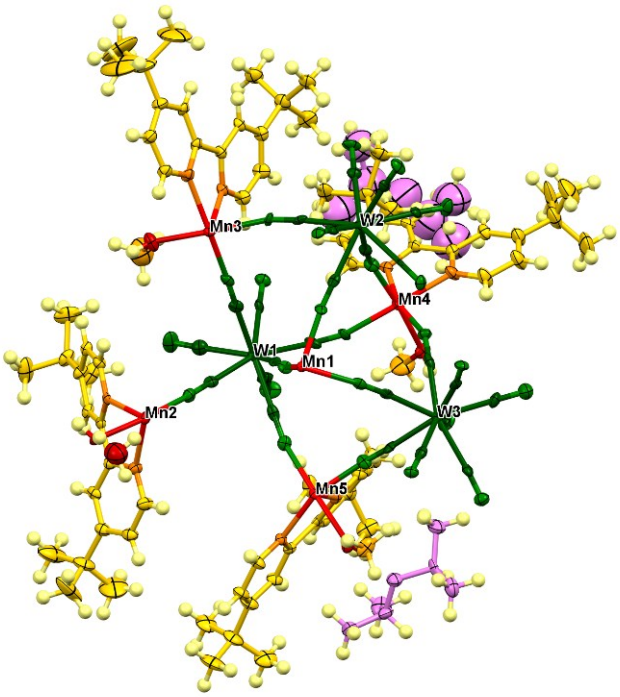

Figure S2. Asymmetric unit of **1a** with atom labelling scheme for metal ions. Atoms spheres are shown with 50% probability ellipsoids. Colours: W, dark green; Mn, red; C of cyanide ligands, green; N of cyanide ligands, light green; N of Bu^t_2bpy ligand, orange, C of Bu^t_2bpy, intense yellow ; H, pale yellow; O of MeOH molecules red; C of MeOH molecules, intense yellow; iPr-O-iPr molecule, magenta.

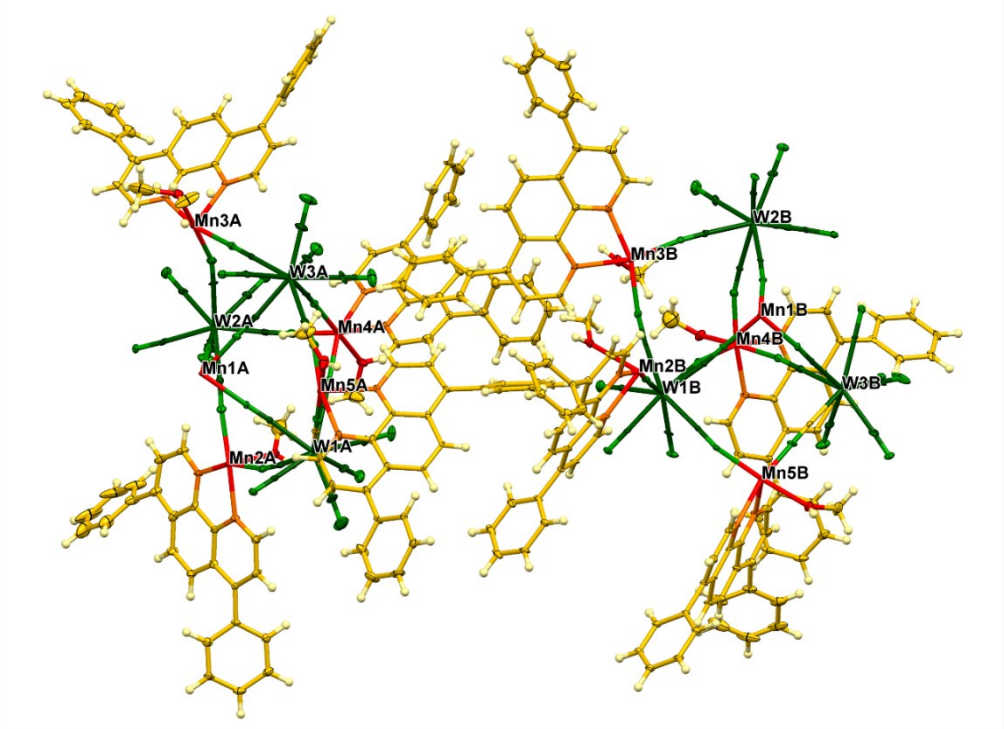

Figure S3. Asymmetric unit of **2** with atom labelling scheme for metal ions. Atoms spheres are shown with 50% probability ellipsoids. Colours: W, dark green; Mn, red; C of cyanide ligands, green; N of cyanide ligands, light green; N of Ph_2phen ligand, orange, C of Ph_2phen, intense yellow ; H, pale yellow; O of MeOH molecules red; C of MeOH molecules, intense yellow.

Table S2. Detailed distances and angles within structure **1**.

Interatomic distances [Å]				Angles [°]			
W1-C11	2.154(7)	Mn1-N11	2.199(6)	W1-C11-N11	175.3(7)	Mn1-N11-C11	170.0(6)
W1-C12	2.159(9)	Mn1-N21	2.188(6)	W1-C12-N12	172.9(8)	Mn1-N21-C21	172.2(6)
W1-C13	2.170(8)	Mn1-N31	2.184(6)	W1-C13-N13	174.9(6)	Mn1-N31-C31	172.0(6)
W1-C14	2.152(9)	Mn2-N12	2.173(7)	W1-C14-N14	175.5(7)	Mn2-N12-C12	161.2(8)
W1-C15	2.161(8)	Mn2-N22	2.169(7)	W1-C15-N15	178.0(6)	Mn2-N22-C22	159.8(7)
W1-C16	2.163(8)	Mn2-N32	2.178(7)	W1-C16-N16	177.4(9)	Mn2-N32-C32	154.5(7)
W1-C17	2.158(9)	Mn2-N41	2.227(7)	W1-C17-N17	178.5(8)	Mn3-N13-C13	164.4(6)
W1-C18	2.157(7)	Mn2-N40A*	2.303(19)*	W1-C18-N18	179.4(8)	Mn3-N23-C23	177.8(7)
W2-C21	2.164(7)	Mn2-N40B*	2.316(19)*	W2-C21-N21	175.4(6)	Mn3-N33-C33	171.5(6)
W2-C22	2.164(8)	Mn2-O1MA*	2.169(18)*	W2-C22-N22	174.2(8)	Mn4-N14-C14	175.8(6)
W2-C23	2.157(8)	Mn2-O1MB*	2.173(18)*	W2-C23-N23	178.4(6)	Mn4-N24-C24	172.5(6)
W2-C24	2.140(8)	Mn3-N13	2.242(7)	W2-C24-N24	178.6(7)	Mn4-N34-C34	164.9(6)
W2-C25	2.167(8)	Mn3-N23	2.164(7)	W2-C25-N25	175.6(6)	Mn5-N15-C15	173.5(7)
W2-C26	2.132(8)	Mn3-N33	2.163(7)	W2-C26-N26	178.4(8)	Mn5-N25-C25	164.4(6)
W2-C27	2.186(9)	Mn3-N60	2.224(6)	W2-C27-N27	177.8(8)	Mn5-N35-C35	173.8(6)
W2-C28	2.172(8)	Mn3-N61	2.243(6)	W2-C28-N28	178.8(8)		
W3-C31	2.162(7)	Mn3-O2M	2.227(6)	W3-C31-N31	175.4(6)		
W3-C32	2.145(8)	Mn4-N14	2.159(7)	W3-C32-N32	173.9(7)		
W3-C33	2.158(8)	Mn4-N24	2.170(7)	W3-C33-N33	179.2(7)		
W3-C34	2.189(8)	Mn4-N34	2.261(7)	W3-C34-N34	175.6(6)		
W3-C35	2.147(7)	Mn4-N80	2.212(6)	W3-C35-N35	176.3(6)		
W3-C36	2.148(9)	Mn4-N81	2.232(6)	W3-C36-N36	179.7(8)		
W3-C37	2.180(9)	Mn4-O3M	2.243(6)	W3-C37-N37	176.4(10)		
W3-C38	2.148(9)	Mn5-N15	2.172(7)	W3-C38-N38	178.3(8)		
		Mn5-N25	2.238(7)				
		Mn5-N35	2.167(7)				
		Mn5-N100	2.240(6)				
		Mn5-N101	2.212(6)				
		Mn5-O4M	2.238(6)				

* - Mn2 site is coordinated by two sets of crystallographically independent MeOH, btbubpy, ligands.

Table S3. Detailed distances and angles within structure **1a**.

Interatomic distances [Å]				Angles [°]			
W1-C11	2.151(10)	Mn1-N11	2.194(8)	W1-C11-N11	175.8(9)	Mn1-N11-C11	169.3(8)
W1-C12	2.148(11)	Mn1-N21	2.181(9)	W1-C12-N12	176.5(8)	Mn1-N21-C21	176.7(8)
W1-C13	2.163(12)	Mn1-N31	2.220(9)	W1-C13-N13	178.5(9)	Mn1-N31-C31	176.8(8)
W1-C14	2.149(12)	Mn2-N12	2.201(9)	W1-C14-N14	176.7(10)	Mn2-N12-C12	164.9(9)
W1-C15	2.162(12)	Mn2-N22	2.137(9)	W1-C15-N15	174.3(9)	Mn2-N22-C22	167.8(9)
W1-C16	2.169(12)	Mn2-N32	2.196(9)	W1-C16-N16	178.7(10)	Mn2-N32-C32	173.7(9)
W1-C17	2.150(13)	Mn2-N40	2.267(9)	W1-C17-N17	178.0(11)	Mn3-N13-C13	172.2(8)
W1-C18	2.171(11)	Mn2-N41	2.218(8)	W1-C18-N18	178.3(9)	Mn3-N23-C23	166.9(9)
W2-C21	2.174(12)	Mn2-O1	2.221(7)	W2-C21-N21	174.8(9)	Mn3-N33-C33	157.2(9)
W2-C22	2.172(11)	Mn3-N13	2.172(9)	W2-C22-N22	178.8(9)	Mn4-N14-C14	175.8(9)
W2-C23	2.200(11)	Mn3-N23	2.271(9)	W2-C23-N23	175.8(9)	Mn4-N24-C24	171.0(8)
W2-C24	2.176(12)	Mn3-N33	2.159(9)	W2-C24-N24	172.6(10)	Mn4-N34-C34	158.4(8)
W2-C25	2.165(12)	Mn3-N60	2.209(8)	W2-C25-N25	177.4(9)	Mn5-N15-C15	173.3(8)
W2-C26	2.162(12)	Mn3-N61	2.247(9)	W2-C26-N26	176.4(9)	Mn5-N25-C25	149.2(9)
W2-C27	2.146(11)	Mn3-O2	2.285(7)	W2-C27-N27	179.3(11)	Mn5-N35-C35	174.2(9)
W2-C28	2.167(11)	Mn4-N14	2.192(9)	W2-C28-N28	176.6(9)		
W3-C31	2.153(11)	Mn4-N24	2.161(9)	W3-C31-N31	176.6(9)		
W3-C32	2.189(12)	Mn4-N34	2.170(9)	W3-C32-N32	172.6(9)		
W3-C33	2.150(12)	Mn4-N80	2.277(9)	W3-C33-N33	178.0(9)		
W3-C34	2.176(12)	Mn4-N81	2.232(8)	W3-C34-N34	174.1(9)		
W3-C35	2.155(12)	Mn4-O3	2.285(7)	W3-C35-N35	176.9(9)		
W3-C36	2.177(11)	Mn5-N15	2.207(9)	W3-C36-N36	173.4(9)		
W3-C37	2.165(12)	Mn5-N25	2.147(9)	W3-C37-N37	174.7(9)		
W3-C38	2.160(12)	Mn5-N35	2.192(9)	W3-C38-N38	177.9(10)		
		Mn5-N100	2.192(8)				
		Mn5-N101	2.244(8)				
		Mn5-O4M	2.256(7)				

Table S4. Detailed distances and angles within cluster A of structure **2**.

Interatomic distances [Å]				Angles [°]			
W1A-C11	2.179(8)	Mn1A-N11A	2.197(7)	W1A-C11-N11	175.8(7)	Mn1A-N11-C11	171.2(7)
W1A-C12	2.165(10)	Mn1A-N21A	2.225(7)	W1A-C12-N12	174.5(7)	Mn1A-N21-C21	172.0(6)
W1A-C13	2.157(9)	Mn1A-N31A	2.225(7)	W1A-C13-N13	178.4(8)	Mn1A-N31-C31	172.3(7)
W1A-C14	2.142(8)	Mn2A-N12A	2.214(9)	W1A-C14-N14	177.9(8)	Mn2A-N12-C12	166.1(7)
W1A-C15	2.160(10)	Mn2A-N22A	2.214(7)	W1A-C15-N15	178.2(8)	Mn2A-N22-C22	174.7(7)
W1A-C16	2.141(10)	Mn2A-N32A	2.255(8)	W1A-C16-N16	177.3(10)	Mn2A-N32-C32	169.9(7)
W1A-C17	2.172(10)	Mn2A-N100	2.268(7)	W1A-C17-N17	178.5(9)	Mn3A-N13-C13	165.1(8)
W1A-C18	2.165(10)	Mn2A-N101	2.261(7)	W1A-C18-N18	176.8(9)	Mn3A-N23-C23	160.7(7)
W2A-C21	2.179(9)	Mn2A-O1M	2.196(6)	W2A-C21-N21	178.4(7)	Mn3A-N33-C33	179.0(7)
W2A-C22	2.170(8)	Mn3A-N13A	2.184(7)	W2A-C22-N22	177.0(8)	Mn4A-N14-C14	177.4(7)
W2A-C23	2.148(9)	Mn3A-N23A	2.242(8)	W2A-C23-N23	177.4(8)	Mn4A-N24-C24	167.7(8)
W2A-C24	2.152(9)	Mn3A-N33A	2.170(8)	W2A-C24-N24	176.6(8)	Mn4A-N34-C34	164.0(7)
W2A-C25	2.160(9)	Mn3A-N200	2.248(7)	W2A-C25-N25	177.6(7)	Mn5A-N15-C15	172.6(7)
W2A-C26	2.162(9)	Mn3A-N201	2.220(7)	W2A-C26-N26	178.1(8)	Mn5A-N25-C25	172.3(8)
W2A-C27	2.182(9)	Mn3A-O2M	2.245(6)	W2A-C27-N27	178.1(10)	Mn5A-N35-C35	168.8(7)
W2A-C28	2.166(10)	Mn4A-N14	2.165(7)	W2A-C28-N28	177.7(10)		
W3A-C31	2.161(8)	Mn4A-N24	2.169(8)	W3A-C31-N31	176.4(7)		
W3A-C32	2.169(9)	Mn4A-N34	2.244(8)	W3A-C32-N32	174.3(7)		
W3A-C33	2.169(9)	Mn4A-N300	2.223(6)	W3A-C33-N33	178.7(9)		
W3A-C34	2.164(9)	Mn4A-N301	2.242(7)	W3A-C34-N34	177.7(7)		
W3A-C35	2.149(9)	Mn4A-O3M	2.248(6)	W3A-C35-N35	177.7(8)		
W3A-C36	2.176(10)	Mn5A-N15	2.210(8)	W3A-C36-N36	179.4(11)		
W3A-C37	2.128(9)	Mn5A-N25	2.168(7)	W3A-C37-N37	179.5(10)		
W3A-C38	2.154(10)	Mn5A-N35	2.139(8)	W3A-C38-N38	178.1(10)		
		Mn5A-N400	2.253(7)				
		Mn5A-N401	2.233(7)				
		Mn5A-O4M	2.241(7)				

Table S5. Detailed distances and angles within cluster B of structure **2**.

Interatomic distances [Å]				Angles [°]			
W1B-C11	2.189(8)	Mn1B-N11A	2.217(6)	W1B-C11-N11	174.7(7)	Mn1B-N11-C11	173.7(7)
W1B-C12	2.172(9)	Mn1B-N21A	2.249(7)	W1B-C12-N12	177.6(7)	Mn1B-N21-C21	170.8(7)
W1B-C13	2.162(8)	Mn1B-N31A	2.249(7)	W1B-C13-N13	175.1(7)	Mn1B-N31-C31	163.1(7)
W1B-C14	2.146(8)	Mn2B-N12A	2.178(8)	W1B-C14-N14	177.7(7)	Mn2B-N12-C12	174.5(7)
W1B-C15	2.177(8)	Mn2B-N22A	2.216(7)	W1B-C15-N15	175.3(7)	Mn2B-N22-C22	162.6(6)
W1B-C16	2.166(9)	Mn2B-N32A	2.182(7)	W1B-C16-N16	179.4(9)	Mn2B-N32-C32	167.1(7)
W1B-C17	2.149(8)	Mn2B-N500	2.236(6)	W1B-C17-N17	177.4(8)	Mn3B-N13-C13	173.6(6
W1B-C18	2.164(8)	Mn2B-N501	2.245(7)	W1B-C18-N18	178.6(7)	Mn3B-N23-C23	164.3(7)
W2B-C21	2.164(8)	Mn2B-O5M	2.298(6)	W2B-C21-N21	177.6(7)	Mn3B-N33-C33	169.7(7)
W2B-C22	2.162(8)	Mn3B-N13A	2.202(7)	W2B-C22-N22	177.7(7)	Mn4B-N14-C14	161.0(7)
W2B-C23	2.188(9)	Mn3B-N23A	2.248(8)	W2B-C23-N23	177.6(7)	Mn4B-N24-C24	162.7(7)
W2B-C24	2.140(8)	Mn3B-N33A	2.250(7)	W2B-C24-N24	176.3(7)	Mn4B-N34-C34	166.8(7)
W2B-C25	2.162(9)	Mn3B-N600	2.275(7)	W2B-C25-N25	177.2(7)	Mn5B-N15-C15	166.4(6)
W2B-C26	2.167(8)	Mn3B-N601	2.248(7)	W2B-C26-N26	179.1(8)	Mn5B-N25-C25	172.5(7)
W2B-C27	2.162(9)	Mn3B-O6M	2.192(7)	W2B-C27-N27	178.3(9)	Mn5B-N35-C35	173.6(7)
W2B-C28	2.168(9)	Mn4B-N14	2.154(7)	W2B-C28-N28	178.8(8)		
W3B-C31	2.169(8)	Mn4B-N24	2.167(7)	W3B-C31-N31	177.3(7)		
W3B-C32	2.148(7)	Mn4B-N34	2.281(7)	W3B-C32-N32	179.7(8)		
W3B-C33	2.178(9)	Mn4B-N700	2.212(7)	W3B-C33-N33	171.2(7)		
W3B-C34	2.173(9)	Mn4B-N701	2.219(7)	W3B-C34-N34	176.0(8)		
W3B-C35	2.153(9)	Mn4B-O7M	2.184(6)	W3B-C35-N35	176.5(7)		
W3B-C36	2.182(9)	Mn5B-N15	2.256(7)	W3B-C36-N36	177.8(8)		
W3B-C37	2.136(10)	Mn5B-N25	2.171(7)	W3B-C37-N37	179.5(11)		
W3B-C38	2.181(9)	Mn5B-N35	2.164(7)	W3B-C38-N38	177.8(8)		
		Mn5B-N800	2.257(7)				
		Mn5B-N801	2.241(6)				
		Mn5B-O8M	2.241(6)				

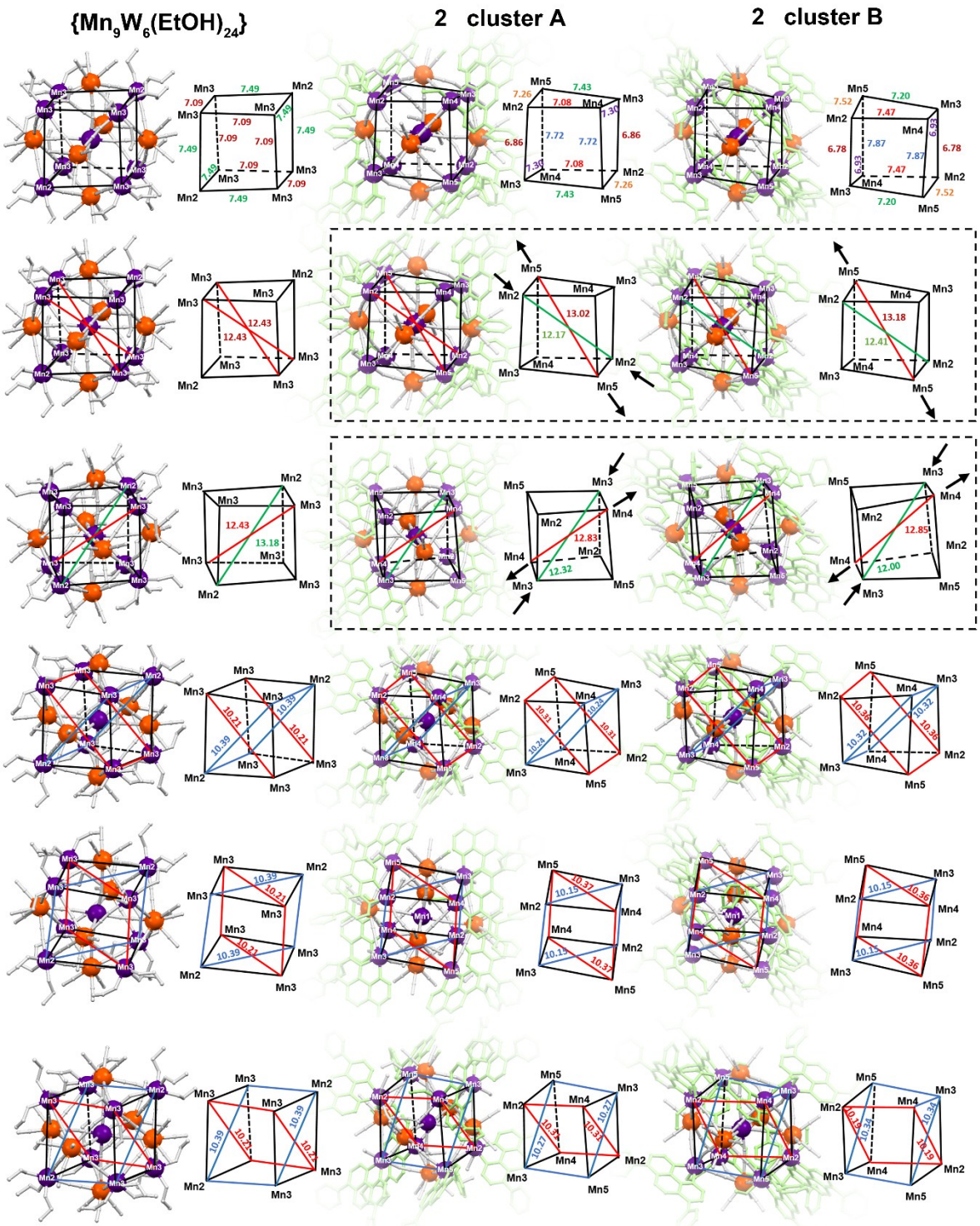

Figure S4. Comparison of Mn_8 super-cube deformation in cluster skeleton. Data for compound $\{Mn_9W_6(EtOH)_{24}\}$ with high symmetry and relatively weak deformation were taken from Zh. J. Zhong et. al work[S1]. The frames indicate elongation of super-polyhedron.

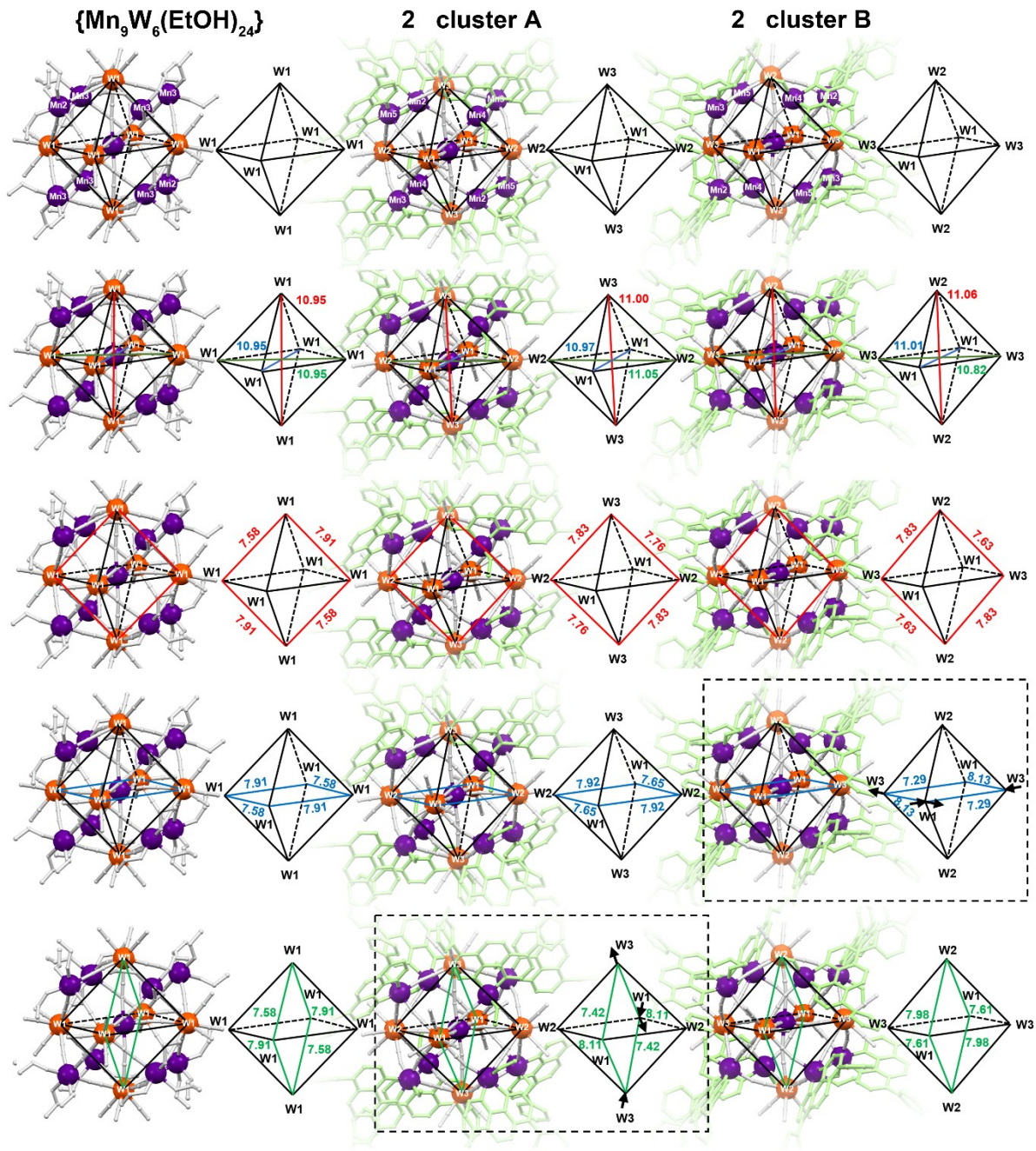

Figure S5. Comparison of W_6 super-octahedron deformation in cluster skeleton. Data for compound $\{Mn_9W_6(EtOH)_{24}\}$ with high symmetry and relatively weak deformation were taken from Zh. J. Zhong et. al work[S1]. The frames indicate elongation of super-polyhedron.

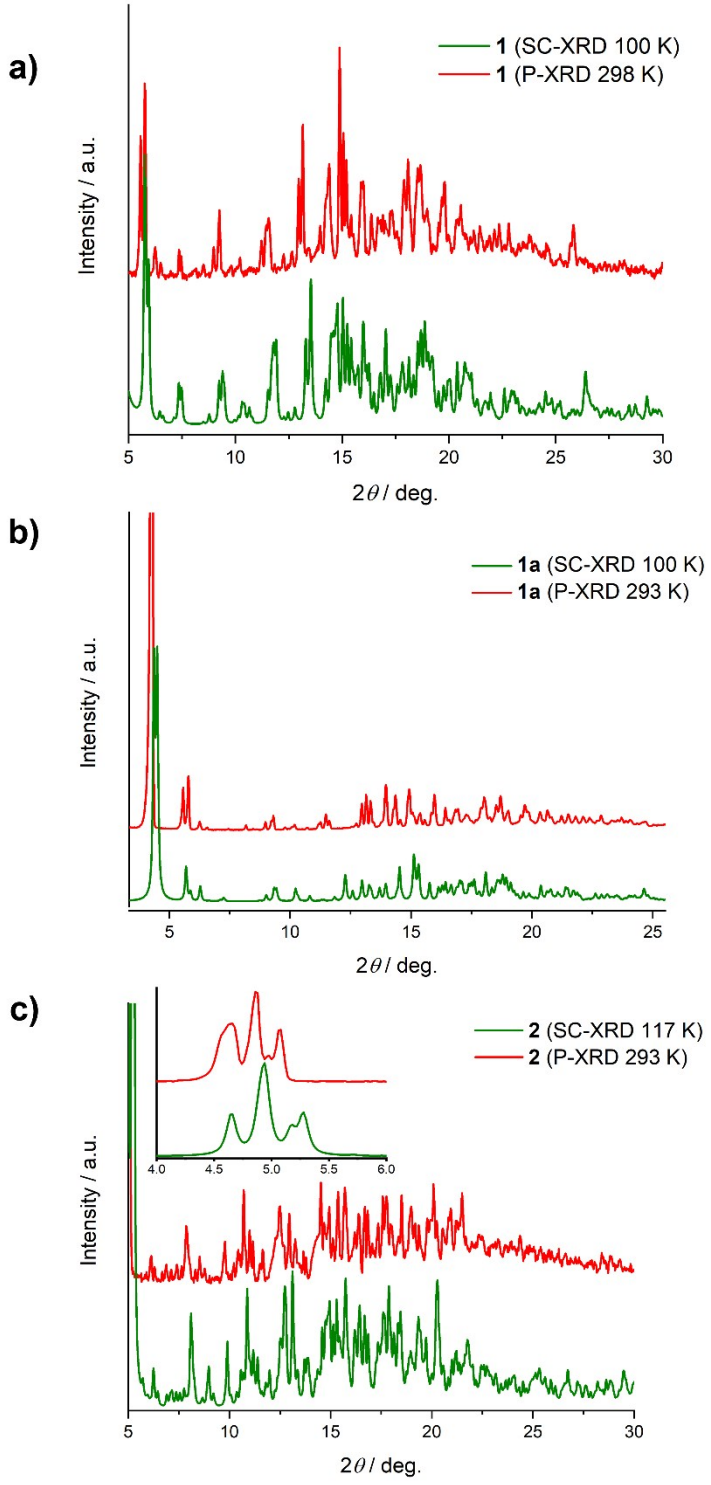

Figure S6. The comparison of experimental (red line) and calculated from SC-XRD model (green line) for **1** (a), **1a** (b) and **2** (c). Experimental patterns were collected using rotating capillary system in mother solution in room temperature. Shift of P-XRD peaks in relation to the calculated from XRD is related to standard temperature effect.

CSM Calculations

Table S6. Results of Continuous Shape Measure Analysis (CSM) for Mn^{2+} sites in **1**,**1a**,**2**.

1	**CSM Parameters**		
	PPY-6	**OC-6**	**TPR-6**
Mn1	29.561	0.222	15.578
Mn2*	25.917	0.956	13.442
Mn2*	26.332	0.877	14.011
Mn3	24.330	0.968	12.064
Mn4	24.439	1.014	12.113
Mn5	24.530	1.069	11.775
1a	**CSM Parameters**		
	PPY-6	**OC-6**	**TPR-6**
Mn1	28.879	0.278	15.553
Mn2	24.123	0.865	13.851
Mn3	25.139	0.835	13.130
Mn4	24.057	1.235	11.100
Mn5	23.038	1.325	11.028
2	**CSM Parameters**		
	PPY-6	**OC-6**	**TPR-6**
Mn1A	29.491	0.066	16.318
Mn2A	25.406	0.995	12.497
Mn3A	24.006	1.089	11.315
Mn4A	22.530	1.065	12.431
Mn5A	26.731	0.578	14.374
Mn1B	29.081	0.132	16.144
Mn2B	25.842	0.967	13.065
Mn3B	25.376	0.985	13.262
Mn4B	26.793	0.550	15.749
Mn5B	25.659	0.820	13.395

* - Mn2 site is coordinated by two sets of crystallographically independent MeOH, btbubpy, ligands.

Polyhedra codes:-

PPY-6 – parameter of pentagonal pyramid geometry related to the C_5V symmetry.

OC-6 – parameter of octahedron geometry related to the Oh symmetry.

TPR-6 – parameter of trigonal prism geometry related to the D_{3h} symmetry.

CSM parameter for ideal geometry equal 0 and increase with distortion from ideal polyhedron.

Table S7. Results of Continuous Shape Measure Analysis (CSM) for $[W(CN)_8]^{3-}$ anions in **1**,**1a**,**2**.

1	**CSM Parameters**		
	SAPR-8	**TDD-8**	**BTPR-8**
W1	1.100	1.619	0.842
W2	1.071	1.602	0.899
W3	0.917	1.659	0.933
1a	**CSM Parameters**		
	SAPR-8	**TDD-8**	**BTPR-8**
W1	1.003	1.531	0.783
W2	1.086	1.627	0.804
W3	0.850	1.056	1.273
2	**CSM Parameters**		
	SAPR-8	**TDD-8**	**BTPR-8**
W1A	1.984	0.524	1.394
W2A	1.179	0.999	1.160
W3A	1.937	0.325	1.612
W1B	0.401	1.803	1.293
W2B	1.117	0.795	1.570
W3B	3.032	0.315	2.031

Polyhedra codes:-

SAPR-8 – parameter of square antiprism geometry related to the D_4d symmetry.

TDD-8 – parameter of triangular dodecaedron geometry related to the D_2d symmetry.

BTPR-8 – parameter of bicapped trigonal prism geometry related to the C_{2v} symmetry.

CSM parameter for ideal geometry equal 0 and increase with distortion from ideal polyhedron.

Table S8. List of intermetallic separation between cluster units for compound **2**.

Type I	12.406Å
Type II	12.505Å
Type II	13.540Å
Type IV	12.000Å
Type V	11.313Å
Type VI	12.966Å
Type VII	13.513Å
Type VIII	9.477Å

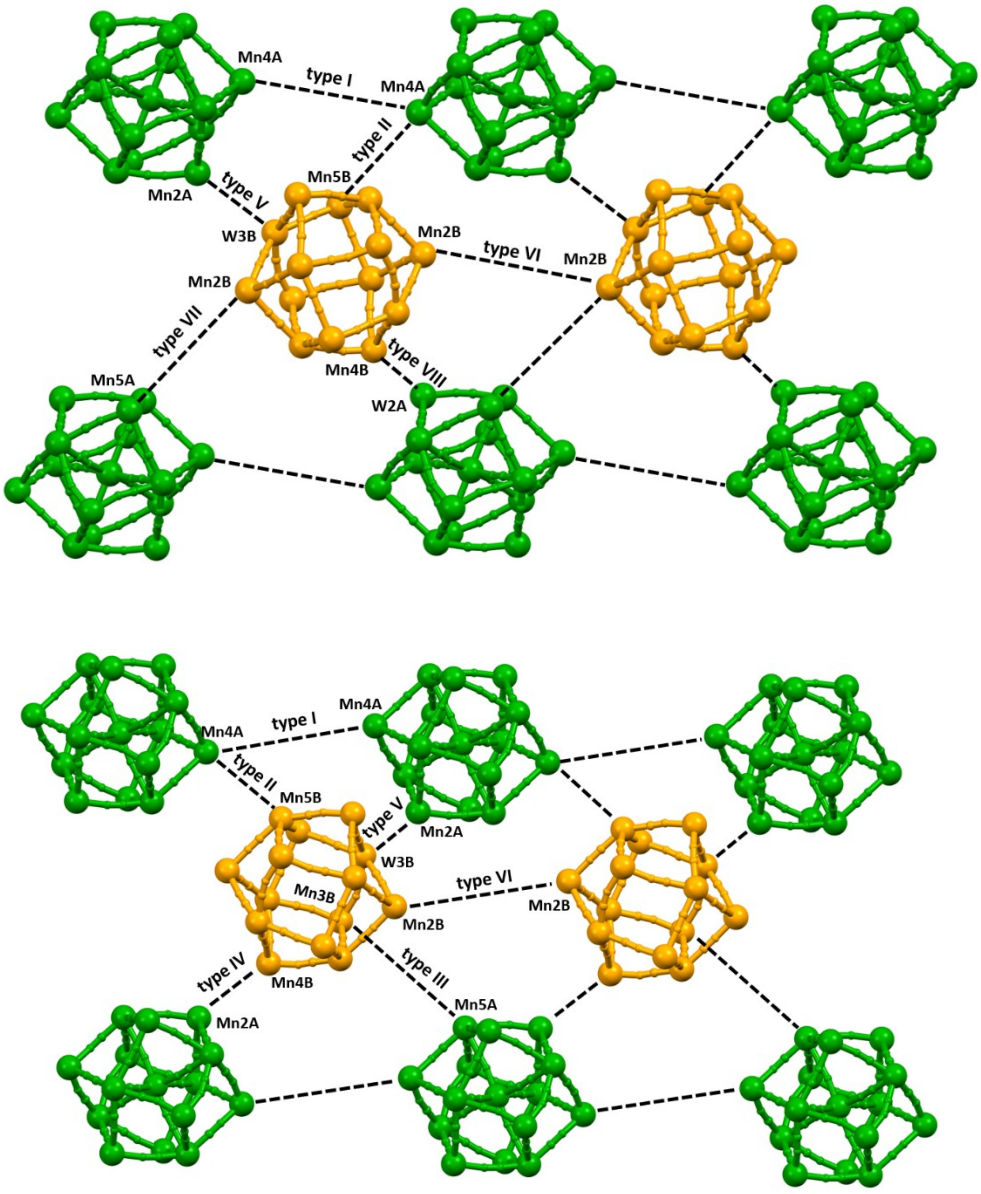

Figure S7. Map of intermetallic separation between cluster units for compound **2**.

II. Magnetic properties

Static magnetic properties

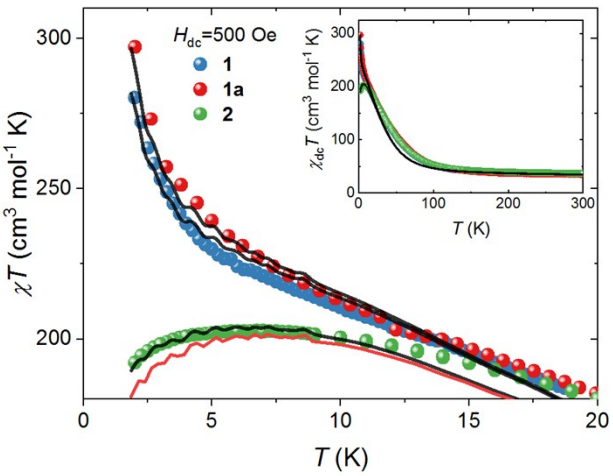

Figure S8. Temperature dependence of χT for **1**, **1a** and **2** as measured at H_{dc}=500 Oe. The temperature dependences of χT are very similar for all compounds from room temperature down to about 20 K. At 300 K the χT values were determined as 36.8, 35.1 and 37.0 cm^3 mol^{-1} K respectively for **1**, **1a** and **2**. Those values are smaller than 41.7 cm^3 mol^{-1} K expected for uncoupled nine Mn^{II} ions (S_{Mn}=5/2, g_{Mn}=2.0) and six W^{V} ions (S_W=1/2, g_W=2.0) which points to non-negligible antiferromagnetic intramolecular interactions at room temperature. Similar behaviour was observed in our previous study of $\{Mn_9[W(CN)_8]_6(4,4'\text{-dpds})_4\}$ and other cyanide-bridge MnW compound.[SI2-SI5] Below 20 K the χT values for each compound diverge as a consequence of intermolecular interactions. The black lines show the fits to eq. 1 (from the main text), while the red line shows the values for isolated cluster $\chi_{iso}T$ with two exchange constants J_{ap}=-8.0 cm^{-1} and J_{eq}=-19.2 cm^{-1} (related to apical and equatorial CN bridges , respectively).

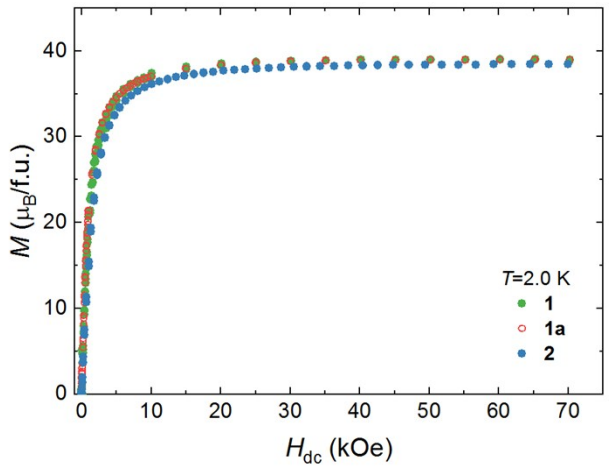

Figure S9. Isothermal magnetization measured at 2.0 K for **1**, **1a** and **2**.

Magnetic relaxation properties

The ac susceptibility as a function of frequency was analyzed with generalized Debye model with one (**1**) and two independent relaxation times (**1a** and **2**). The formula for one relaxation process is given by formula:

$$\chi(\omega) = \chi_S + \frac{(\chi_T - \chi_S)}{1 + (i\omega\tau)^{1-\alpha}} \qquad \text{(eq. S1)},$$

while the equation for two relaxation times take form:

$$\chi(\omega) = \chi_S + (\chi_T - \chi_S)\left[\frac{\beta}{1 + (i\omega\tau_1)^{1-\alpha_1}} + \frac{1-\beta}{1 + (i\omega\tau_2)^{1-\alpha_2}}\right], \qquad \text{(eq. S2)}.$$

In both equations (eq. S1 and eq. S2) χ_S is the adiabatic susceptibility, χ_T is the isothermal susceptibility, $\omega=2\pi f$ is the angular frequency, τ, τ_1 and τ_2 are the relaxation times, α, α_1 and α_2 (values from 0 to 1) are the distributions of the relaxation processes, β (values from 0 to 1) is the relative weight of the susceptibility change related to first relaxation process (τ_1) whereas the 1-β is related with the second relaxation process (τ_2).

The real part and the imaginary part for single relaxation time are given by (eq. S3) and (eq. S4), respectively.

$$\chi' = \chi_S + \frac{(\chi_T - \chi_S)[1 + (\omega\tau)^{1-\alpha}\sin(1/2\alpha\pi)]}{1 + 2(\omega\tau)^{1-\alpha}\sin(1/2\alpha\pi) + (\omega\tau_1)^{2(1-\alpha)}} \qquad \text{(eq. S3)}$$

$$\chi'' = \frac{(\chi_T - \chi_S)(\omega\tau)^{1-\alpha}\cos(1/2\alpha\pi)}{1 + 2(\omega\tau)^{1-\alpha}\sin(1/2\alpha\pi) + (\omega\tau)^{2(1-\alpha)}} \qquad \text{(eq. S4)}$$

In case of two relaxation processes the real part and the imaginary part are given by Eq. (S5) and Eq. (S6), respectively.

$$\chi' = \chi_S + (\chi_T - \chi_S)\times \left\{\frac{\beta[1 + (\omega\tau_1)^{1-\alpha_1}\sin(1/2\alpha_1\pi)]}{1 + 2(\omega\tau_1)^{1-\alpha_1}\sin(1/2\alpha_1\pi) + (\omega\tau_1)^{2(1-\alpha_1)}} + \frac{(1-\beta)[1 + (\omega\tau_2)^{1-\alpha_2}\sin(1/2\alpha_2\pi)]}{1 + 2(\omega\tau_2)^{1-\alpha_2}\sin(1/2\alpha_2\pi) + (\omega\tau_2)^{2(1-\alpha_2)}}\right\} \qquad \text{(eq. S5)}$$

$$\chi'' = (\chi_T - \chi_S)\left\{\frac{\beta(\omega\tau_1)^{1-\alpha_1}\cos(1/2\alpha_1\pi)}{1 + 2(\omega\tau_1)^{1-\alpha_1}\sin(1/2\alpha_1\pi) + (\omega\tau_1)^{2(1-\alpha_1)}} + \frac{(1-\beta)(\omega\tau_2)^{1-\alpha_2}\cos(1/2\alpha_2\pi)}{1 + 2(\omega\tau_2)^{1-\alpha_2}\sin(1/2\alpha_2\pi) + (\omega\tau_2)^{2(1-\alpha_2)}}\right\} \text{(eq.S6)}$$

The in-phase (χ') and out-of-phase (χ'') components of ac susceptibility were fitted simultaneously.

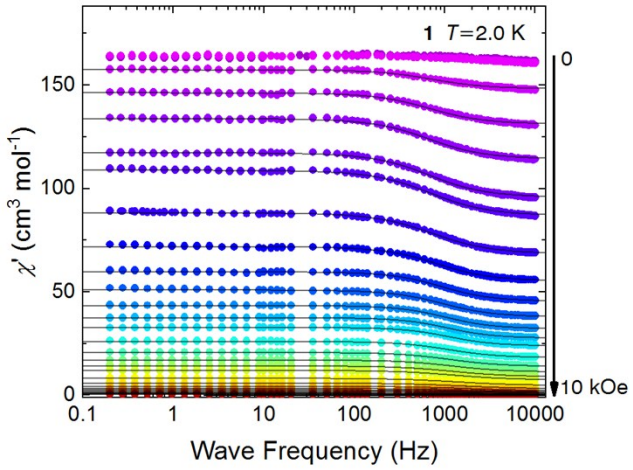

Figure S10. Frequency dependence of in-phase ac susceptibility (χ') in dc field range: 0 - 10 kOe at 2.0 K for **1**. The solid lines correspond to the extended Debye model fits.

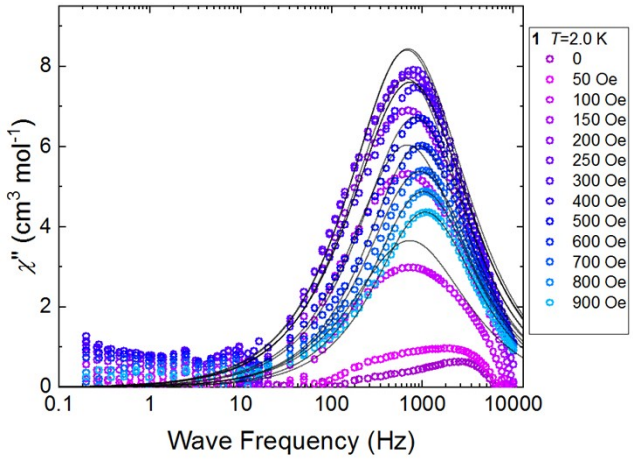

Figure S11. Frequency dependence of out-of-phase ac susceptibility (χ'') in dc field range: 0 - 900 Oe at 2.0 K for **1**. The solid lines correspond to the extended Debye model fits.

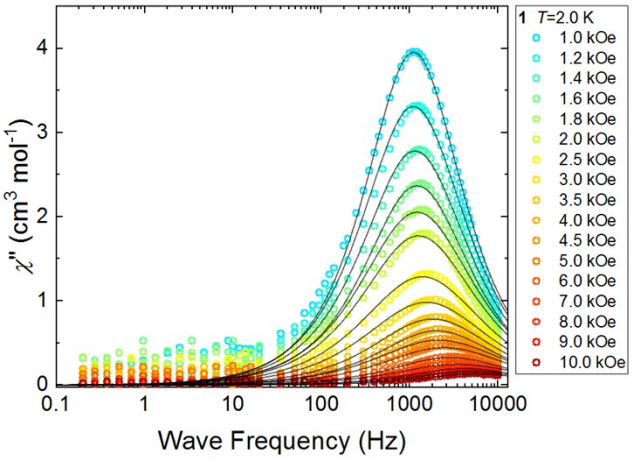

Figure S12. Frequency dependence of out-of-phase component of ac susceptibility (χ'') in dc field range: 1 – 10 kOe at 2.0 K for **1**. The solid lines correspond to the extended Debye model fits.

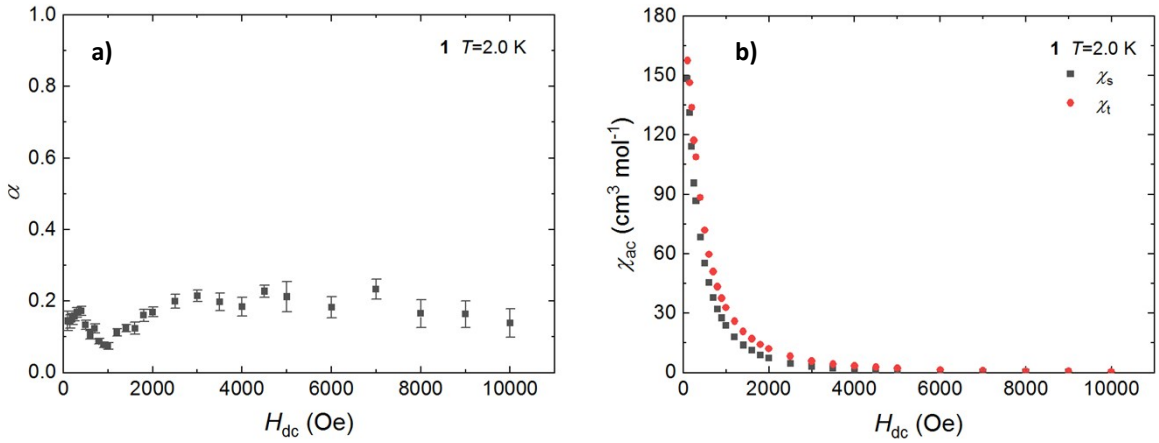

Figure S13. a) dc field dependence of α parameter at 2.0 K for **1**. **b)** dc field dependence of the adiabatic susceptibility χ_s (black squares) and isothermal susceptibility χ_t (red circles) at 2.0 K for **1**.

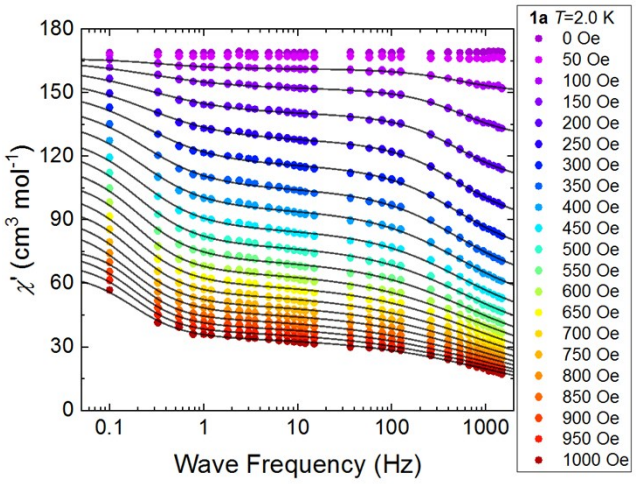

Figure S14. Frequency dependence of in-phase ac susceptibility (χ') in dc field range: 0 - 1 kOe at 2.0 K for **1a**. The solid lines correspond to the extended Debye model fits.

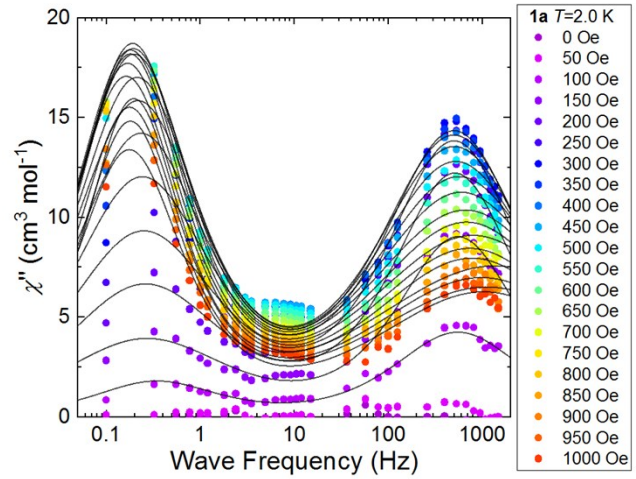

Figure S15. Frequency dependence of out-of-phase ac susceptibility (χ'') in dc field range: 0 - 1 kOe at 2.0 K for **1a**. The solid lines correspond to the extended Debye model fits.

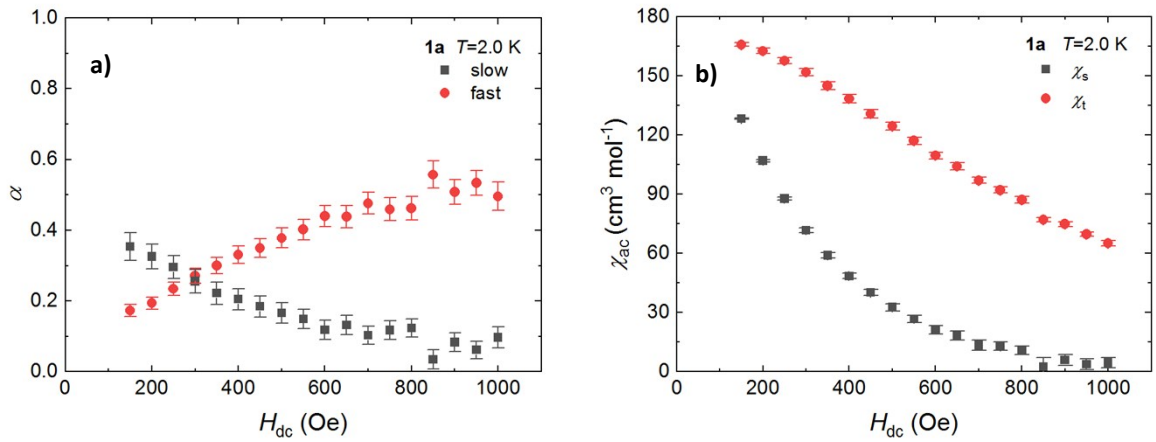

Figure S16. a) dc field dependence of α parameter at 2.0 K for **1a**. **b)** dc field dependence of the adiabatic susceptibility χ_s (black squares) and isothermal susceptibility χ_t (red circles) at 2.0 K for **1a**.

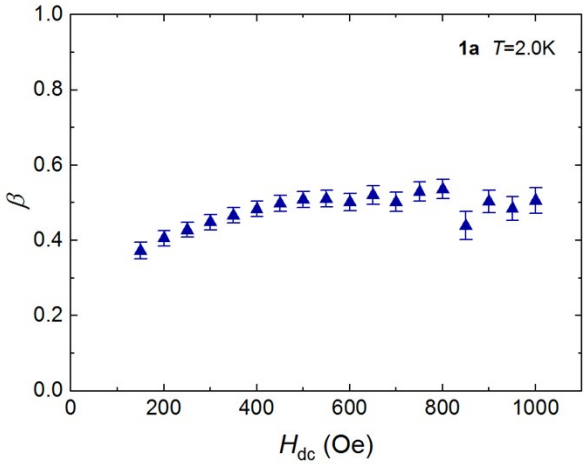

Figure S17. dc field dependence of the weight of the slow relaxation process β at 2.0 K for **1a.**

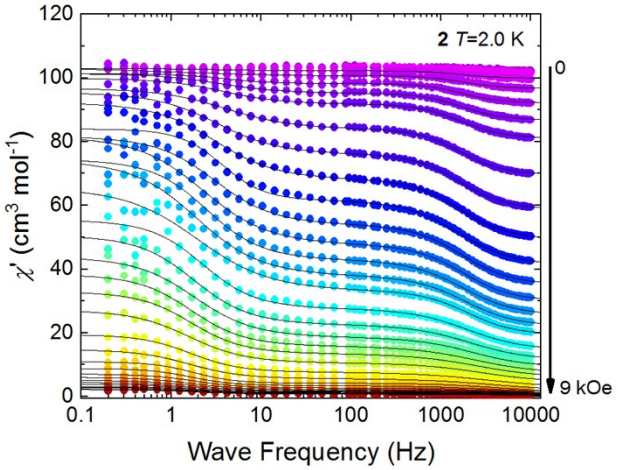

Figure S18. Frequency dependence of in-phase ac susceptibility (χ') in dc field range: 0 – 9 kOe at 2.0 K for **2**. The solid lines correspond to the extended Debye model fits.

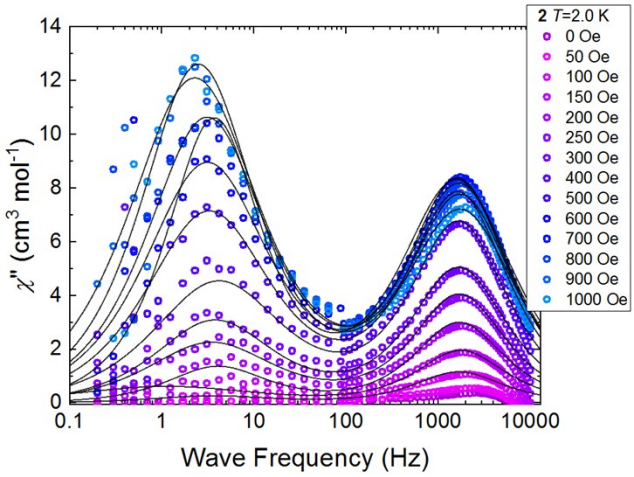

Figure S19. Frequency dependence of out-of-phase ac susceptibility (χ'') in dc field range: 0 - 1000 Oe at 2.0 K for **2**. The solid lines correspond to the extended Debye model fits.

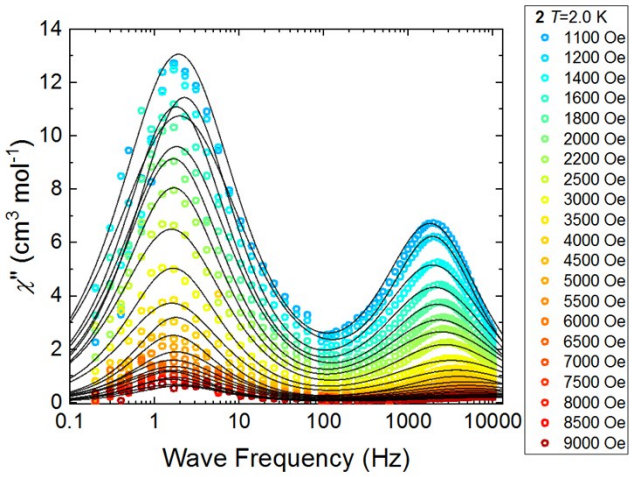

Figure S20. Frequency dependence of out-of-phase ac susceptibility (χ'') in dc field range: 1100 - 9000 Oe at 2.0 K for **2**. The solid lines correspond to the extended Debye model fits.

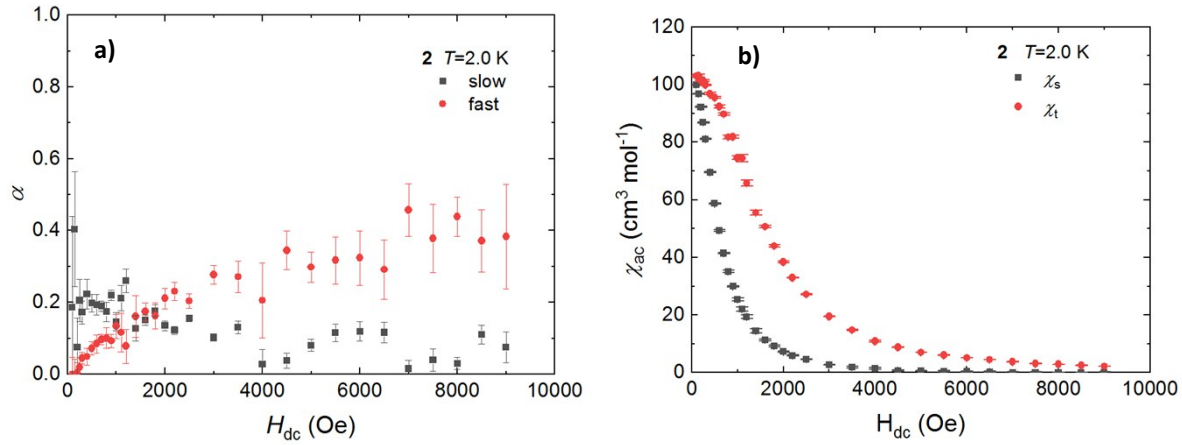

Figure S21. a) dc field dependence of α parameter at 2.0 K for **2**. **b**) Black squares correspond to slow relaxation process ($\tau_{2\text{-slow}}$) , while red circles to the fast relaxation time ($\tau_{2\text{-fast}}$).

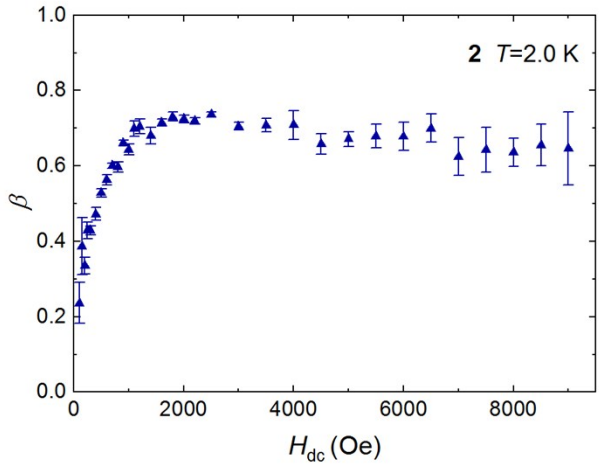

Figure S22. dc field dependence of the weight of the slow relaxation process β at 2.0 K for **2**.

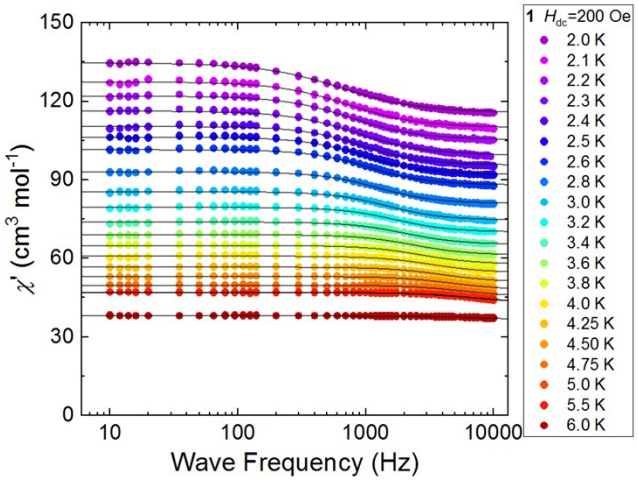

Figure S23. Frequency dependence of in-phase ac susceptibility (χ') with applied field of 200 Oe in temperature range: 2.0 K - 6.0 K for **1**. The solid lines correspond to the extended Debye model fits.

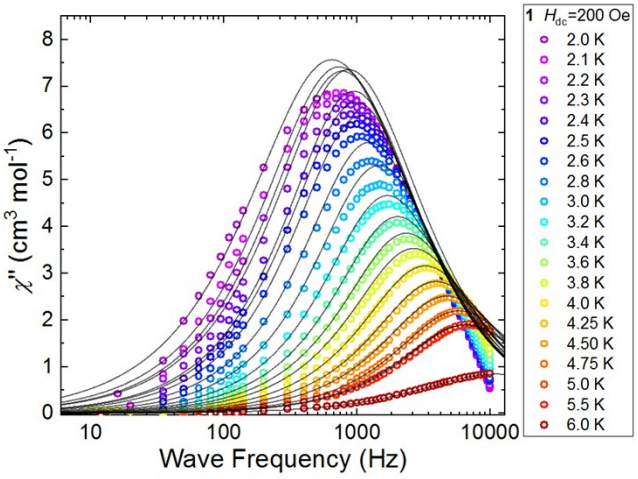

Figure S24. Frequency dependence of out-of-phase ac susceptibility (χ'') with applied field of 200 Oe in temperature range: 2.0 K - 6.0 K for **1**. The solid lines correspond to the extended Debye model fits.

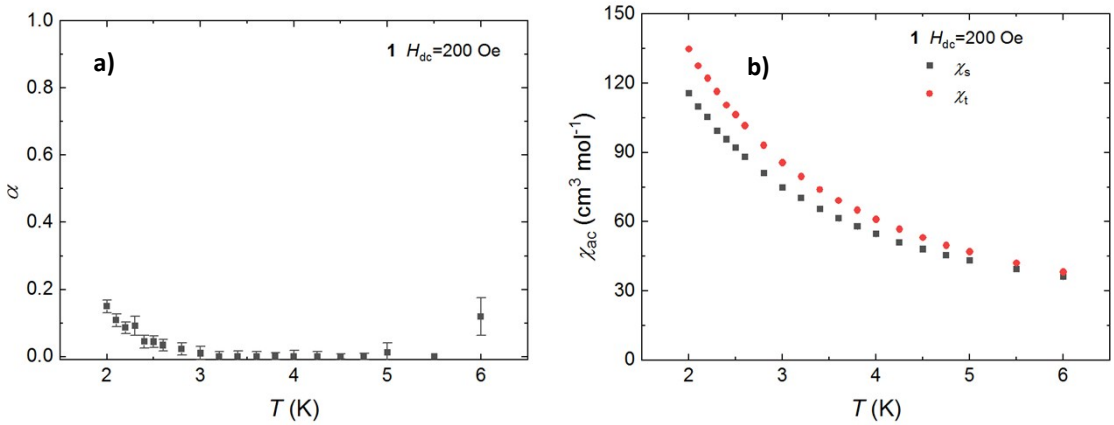

Figure S25. a) Temperature dependence of α parameter with applied field of 200 Oe for **1**. **b**) Temperature dependence of the adiabatic susceptibility χ_s (black circles) and isothermal susceptibility χ_t (red circles) at 200 Oe for **1**.

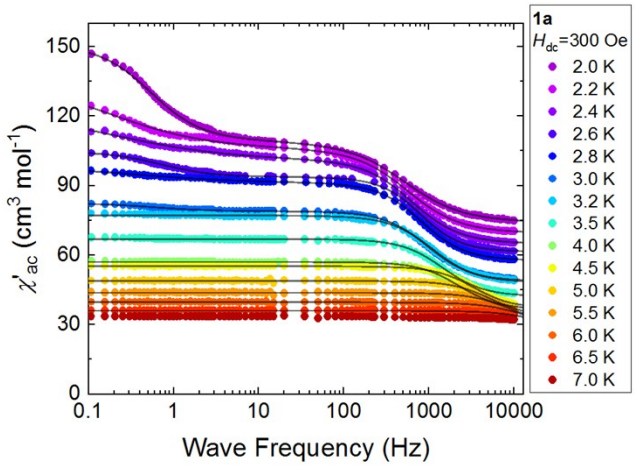

Figure S26. Frequency dependence of in-phase ac susceptibility (χ') with applied field of 300 Oe in temperature range: 2.0 K - 7.0 K for **1a**. The solid lines correspond to the extended Debye model fits.

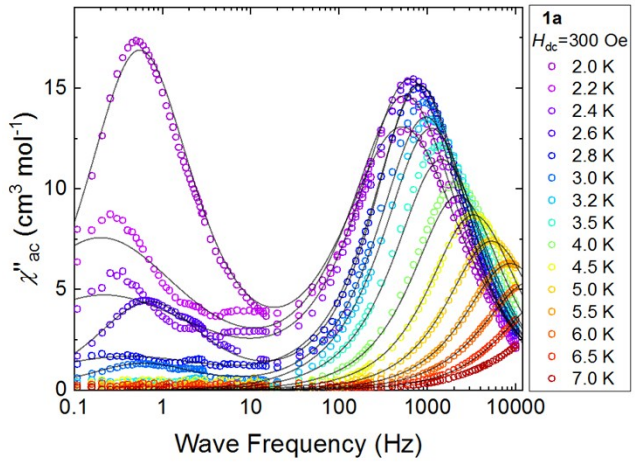

Figure S27. Frequency dependence of out-of-phase ac susceptibility (χ'') with applied field of 300 Oe in temperature range: 2.0 K - 7.0 K for **1a**. The solid lines correspond to the extended Debye model fits.

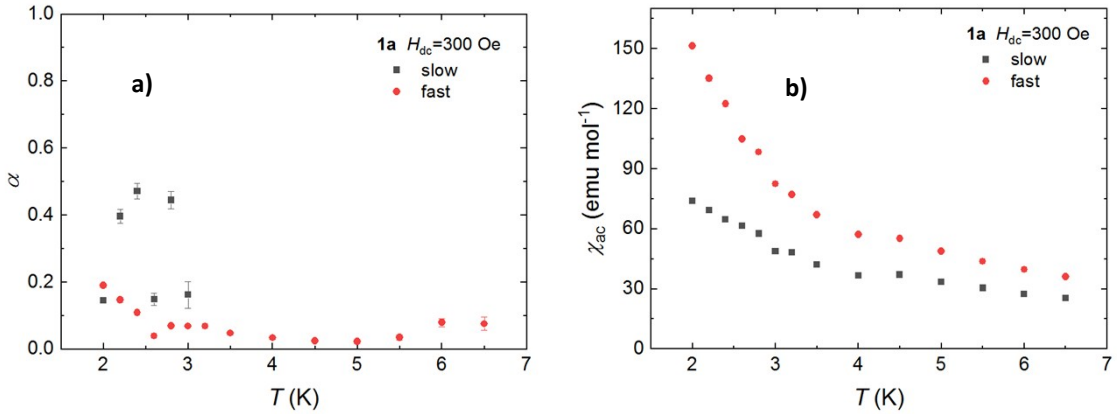

Figure S28. a) Temperature dependence of α parameter with applied field 300 Oe for **1a**. Black squares correspond to slow relaxation process ($\tau_{2\text{-slow}}$) , while red circles to the fast relaxation time ($\tau_{2\text{-fast}}$). **b)** Temperature dependence of the adiabatic susceptibility χ_s (black squares) and isothermal susceptibility χ_t (red circles) at 300 Oe for **1a**.

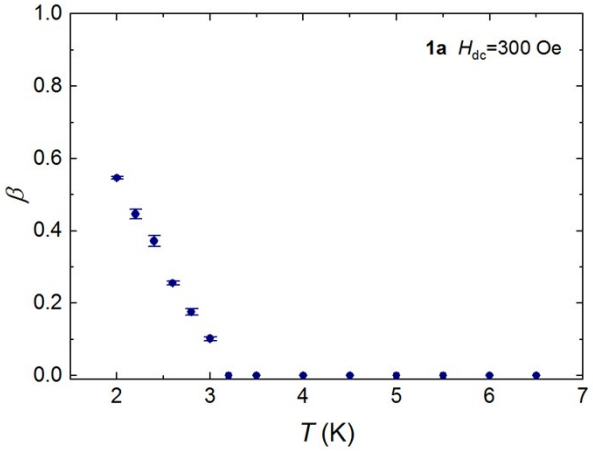

Figure S29. Temperature dependence of the weight of the slow relaxation process β in applied field 300 Oe for **1a**.

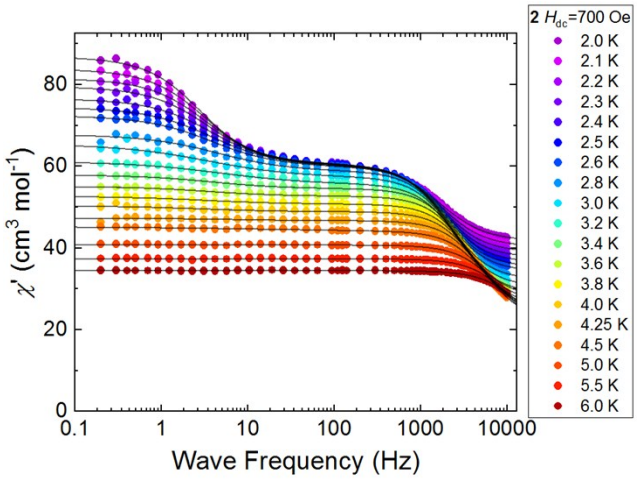

Figure S30. Frequency dependence of in-phase ac susceptibility (χ') with applied field of 700 Oe in temperature range: 2.0 K - 6.0 K for **2**. The solid lines correspond to the extended Debye model fits.

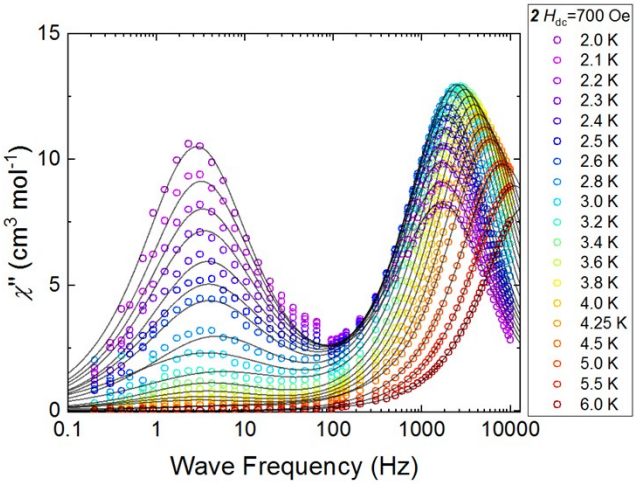

Figure S31. Frequency dependence of out-of-phase ac susceptibility (χ'') with applied field of 700 Oe in temperature range: 2.0 K - 6.0 K for **2**. The solid lines correspond to the extended Debye model fits.

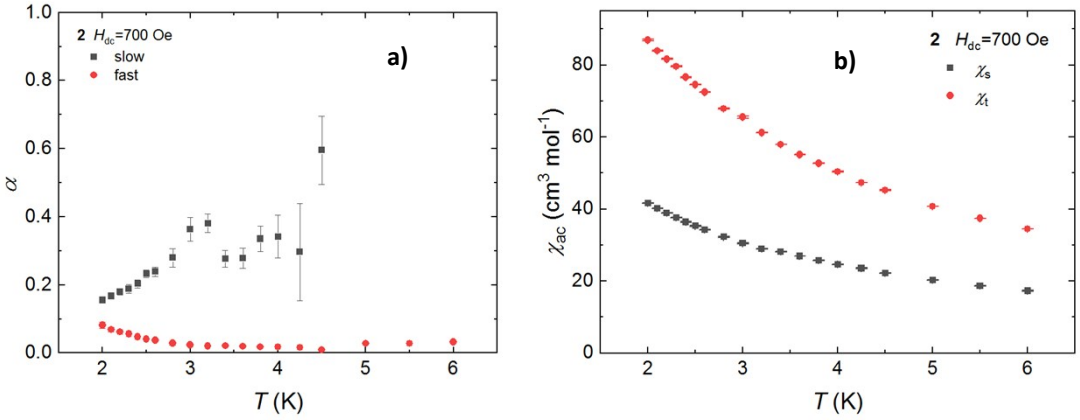

Figure S32. a) Temperature dependence of α parameter for the slow relaxation time (black squares) and fast relaxation time (red circles) in applied field of 700 Oe for **2**. **b**) Temperature dependence of the adiabatic susceptibility χ_s (black squares) and isothermal susceptibility χ_t (red circles) at 700 Oe for **2**.

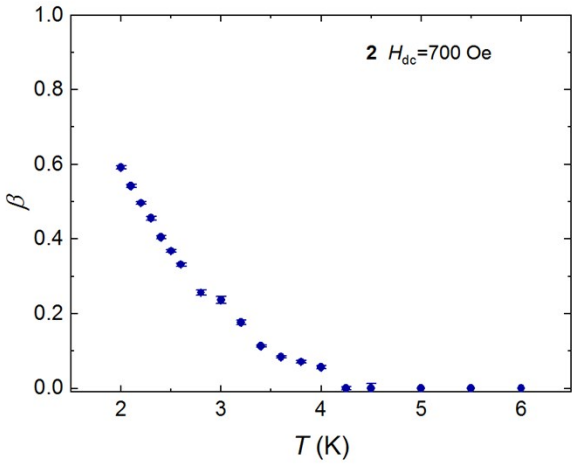

Figure S33. Temperature dependence of the weight of the slow relaxation process β in applied field of 700 Oe for **2**.

S1. Zh. J. Zhong, S., Hidetake. Y. Mizobe, M. Hidai, A. Fujishima, S. Ohkoshi, K. Hashimoto, Kazuhito, J. Am. Chem. Soc. 2000, 122, 2952-2953.

S2. D. Pinkowicz, R. Podgajny, B. Nowicka, S. Chorazy, M. Reczynski, B. Sieklucka, *Inorg. Chem. Front.* **2015,***2*, 10-27.

S3. P. Konieczny, S. Chorazy, R. Pełka, K. Bednarek, T. Wasiutyński, S. Baran, B. Sieklucka, R. Podgajny, *Inorg. Chem.* **2017,***56*, 7089-7098.

S4. B. Nowicka, T. Korzeniak, O. Stefańczyk, D. Pinkowicz, S. Chorąży, R. Podgajny, B. Sieklucka, *Coord. Chem. Rev.* **2012,***256*, 1946-1971.

S5. Y.-Q. Zhang, C.-L. Luo, *Dalton, Trans.* 2008, 4575-4584.